

The Intraseasonal Oscillation in Eastern Pacific Sea Levels: How Is It Forced?

DAVID B. ENFIELD*

College of Oceanography, Oregon State University, Corvallis, OR 97331

(Manuscript received 24 October 1986, in final form 11 February 1987)

ABSTRACT

Daily sea level and surface winds at eastern Pacific shore locations and equatorial islands, together with gridded five-day averages of 850 mb winds, have been analyzed for the 1979–84 period to determine how the 40–60 day intraseasonal oscillation of eastern Pacific sea levels is forced, as described by Spillane et al. for 1971–75. The oscillation was also present in 1980–84 from Callao, Peru, to San Francisco, with maximum energy near 52–57 days and band limits of 43 and 65 days. During 1980–84 there was no evidence for forcing of the large-scale oscillation in the eastern Pacific, although a local contribution of forcing was superimposed on the remote signal at the California stations. Interannual fluctuations in amplitude were evident in the sea level time series, consistent with those of the corresponding wind oscillation in the western equatorial Pacific. The oscillation was best developed in both variables in 1980–82 and became weak or nonexistent during the recovery phase of the 1982–83 El Niño, similar to a weakening that occurred following the 1972–73 episode, noted by Spillane et al. The sea level oscillations have the characteristics of lowest baroclinic mode Kelvin waves that are primarily forced by a similar, energetic oscillation in the winds in the western equatorial Pacific. During the 1980–82 period a significant component of the wind signal extended into the central Pacific and was associated with sea level propagation speeds of about 5 m s^{-1} , suggesting a more extensive forcing along the equatorial waveguide at that time. In 1982–84, when the oscillation was weak, the sea level propagation was about 3 m s^{-1} , consistent with the free propagation of lowest baroclinic mode Kelvin waves in the central Pacific.

1. Introduction

This paper is a sequel to the recent work of Spillane et al. (1987, henceforth SEA), which for the first time fully documents the large scale, coherent and poleward propagating nature of an ubiquitous 40–60 day oscillation in 1971–75 eastern Pacific sea levels that ranges at least from central Peru to northern California. The SEA analysis of this intraseasonal oscillation failed to find sources of local or regional forcing along the eastern boundary. This paper extends the search for energy, coherence, propagation and forcing to the equatorial Pacific, to see if the oceanic oscillation is related to its well-known atmospheric counterpart, where and in what way.

The similar, but wider-band, oscillation in the atmospheric troposphere was serendipitously discovered about 15 years ago (Madden and Julian, 1971, 1972). Since then, this intraseasonal oscillation has been extensively observed in the fields of outgoing longwave radiation (OLR, related to deep convection anomalies) and in the high and low-level zonal tropospheric circulations (e.g., Weickmann et al., 1985; Knutson and Weickmann, 1987). The oscillation phenomenon is most frequently ascribed to equatorially trapped atmospheric Kelvin waves that are excited by convective disturbances between about 60°E and 160°E , where the signal is also most intense (Parker, 1973; Chang, 1977; Lau and Peng, 1987). The associated anomalies

tend to be concentrated within about 20° of the equator and propagate eastward around the globe at $5\text{--}15 \text{ m s}^{-1}$ with a wavelength of one earth circumference. Thus, the anomalies in the Indonesian convective region are 180 degrees out of phase with those in a similar area of more intense tropical convection over northeast Brazil and the western equatorial Atlantic, on the opposite side of the globe. The propagation is not uniform, however, in either space or time; it is well defined over the regions and time periods for which the oscillation activity is most intense (Murakami et al., 1986). Accordingly, phase has a more propagating (stationary) nature over the eastern (western) hemisphere. The 850 mb winds fluctuate in quadrature with the OLR (vertical motion) phases reported by others. Typically, when a negative OLR anomaly (strong convection) lies over Indonesia, a positive anomaly (weak convection, or subsidence) lies near the dateline and the low level winds between the two regions are in an easterly phase. Meridional phase propagation from the equatorial region to higher latitudes has also been detected, especially from the Indian Ocean northward into the Indian subcontinent (Murakami et al., 1986).

The oscillations are not strictly periodic, but have a preferred time scale of 30–60 days, which has been attributed to the time it takes the atmospheric Kelvin waves to circuit the globe (Lau and Peng, 1987). The period range most often cited for the oscillation is 40–50 days (Anderson et al., 1984), but the observed periodicities vary from 25 days (Parker, 1973) to 90 days (Weickmann, 1983). In the western equatorial Pacific,

* Present affiliation: NOAA/Atlantic Oceanographic and Meteorological Laboratory, Miami, FL 33149.

neither the amplitude nor the period undergoes a detectable annual modulation but both are seen to vary at erratic intervals on the order of a season or more (Anderson et al., 1984). Murakami et al. (1986) found that strong interannual modulations of 2–3 years occur in the oscillation amplitude, apparently caused by a beat between twin spectral peaks. They noted large amplitudes and well-defined eastward propagation in the eastern hemisphere during 1981–82; the same characteristics were weak or absent in 1983. They also noted subtle seasonal differences in the zonal propagation, which appears to be better defined during the boreal summer.

Bits and pieces of the sea level signal have been reported more recently by oceanographers. Picaut and Verstraete (1976) found a strong, spatially coherent 40–50 day stationary oscillation in coastal sea levels and sea surface temperatures (SSTs) in the Gulf of Guinea, which they presumed to be forced in some way by the counterpart wind oscillation in the atmosphere. Luther (1980) found a 35–80 day propagating signal in equatorial Pacific island sea level records. Somewhat later, Mysak and Mertz (1984) and Mertz and Mysak (1984) noted an oceanic oscillation in data from the Somali Current region, and Breaker and Lewis (1988) from shore temperatures in central California. Finally, Enfield and Lukas (1984) observed that a 45-day periodicity in Peru sea level is well correlated at large lags with the intraseasonal oscillation in western Pacific zonal winds. What has been lacking in such studies is an analysis of both atmospheric and oceanic data on a basinwide, multiannual scale, in order to establish the structure of the oscillation in both media as well as their mutual relations.

In the SEA analysis, five years of sea level height (SLH) data were examined for 19 tide stations from Callao, Peru (12°S) to Prince Rupert, Canada (54°N) for the period 1971–75. A strong ridge of 40–60 day spectral energy in latitude–frequency space extends from Callao to the Gulf of California, and a corresponding ridge in coherence extends onward to central-northern California. Frequency domain analysis of empirical orthogonal functions (FDEOFs) within the 40–60 day band reveal characteristic large-scale coherence and phase structures that are seasonally invariant and have a clear phase propagation of 150–200 km day⁻¹ from the near-equatorial region to northern California. Within 5–10 degrees of the equator the amplitude of the signal is considerably smaller, consistent with the conservation of alongshore energy flux in a coastal Kelvin wave with small dissipation. The low-latitude phase propagation is considerably faster, consistent with theoretical expectations for coastal-trapped waves of low frequency (Cane and Sarachik, 1977). An abrupt decrease in amplitude (but not coherence) occurs at the California stations, attributed to energy dissipation in the Gulf of California. Available wind data from points close to the Northern

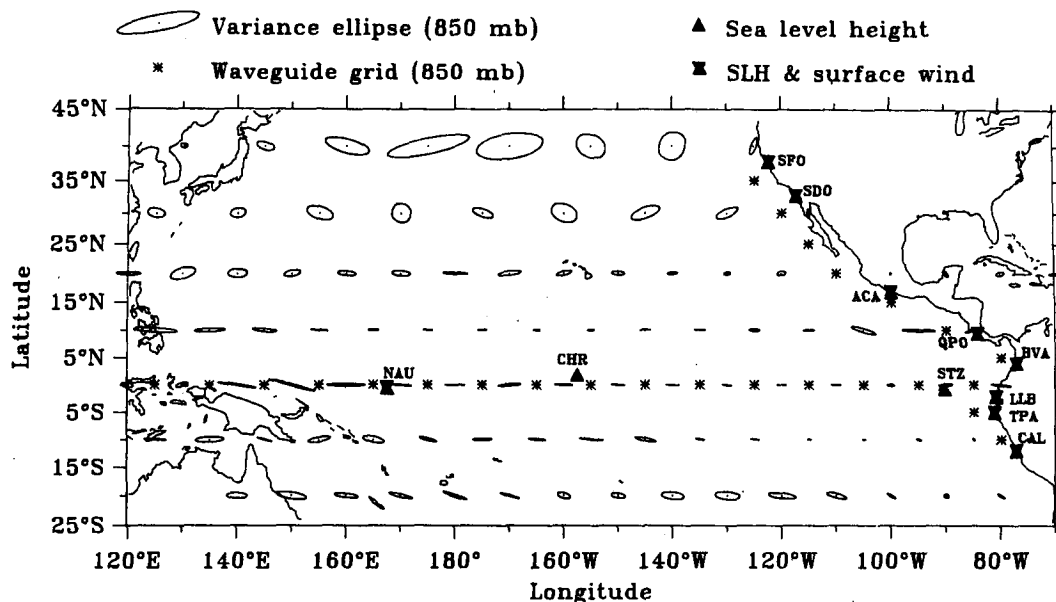
Hemisphere tide stations show little or no coherence with the spatially organized FDEOF signal in SLH, suggesting that the sea level variability is remotely forced and travels along the eastern boundary as freely propagating coastal-trapped waves.

In the present analysis, special emphasis is placed on tracing the source of the 40–60 day SLH signal, guided by the hypothesis that it is forced by its well-known atmospheric counterpart, and using datasets for the period 1979–84 whose distributions are shown in Fig. 1. We will show that the oscillation in eastern Pacific sea levels is forced in the western and central equatorial Pacific and propagates eastward along the equator to South America. There the signal continues poleward into both hemispheres and is unforced, in agreement with SEA. The equatorial sea level signal is interannually nonstationary in its strength and phase speed, in accordance with indications that the forcing varies in its intensity and zonal extent.

2. Data

Six years (1979–84) of tide and atmospheric data for the stations listed in Table 1 have been obtained and processed for analysis. Original tabulations of hourly tide heights for the coastal stations were copied and later digitized, then checked for datum shifts using the staff comparison readings and leveling data also provided by the source agencies. The data were further screened for errors and datum shifts by comparing the hourly observations with tidal predictions or by examining time series formed by differencing between neighboring stations. Short gaps of up to a few days in length were bridged by applying an autoregressive prediction filter based on the data before and after each gap. Finally, the series were smoothed using a cosine-Lanczos filter with an amplitude response of 10%, 50% and 90% at periods of 30, 40 and 60 h, and the data decimated to once-daily values at Greenwich noon. Similarly processed SLH series were obtained from the University of Hawaii for three equatorial islands: Nauru (167°E), Christmas (158°W) and Santa Cruz (90°W) (courtesy K. Wyrcki).

Several gaps at Nauru and Santa Cruz Islands were filled by regression on data from nearby Tarawa and Isabela (Galapagos) Islands, respectively. The 1982–85 data from a tide gauge installed at Paita, Peru (5°S) under the Equatorial Pacific Ocean Climate Studies (EPOCS) program was spliced by regression to the highly coherent 1979–81 data from Talara (less than 50 km to the north), which subsequently deteriorated badly in quality and continuity. We refer to the combined series as Talara–Paita (TPA). A one-month gap at Talara–Paita (March 1980) was filled by regression on La Libertad. This is the only instance where predictor data is also used in the analysis but, since the gap is only a few percent of the total data duration, the artificial coherence introduced is minimal.



Data Grids and Station Locations

FIG. 1. Locations of sea level stations and surface wind data, a 25-point grid for 850 mb winds over the equatorial and coastal waveguides and a 102-point large scale grid of 850 mb winds. Principal axis variance ellipses for the 40-57 day band are plotted at the large-scale grid points. Station abbreviations are defined in Table 1.

Surface wind data for coastal and island locations comes from several sources (Table 1). For points near the Northern Hemisphere (coastal) tide stations, we use the geostrophic wind stress derived from gridded atmospheric pressure data provided by the Fleet Numerical Oceanography Center (FNOC), also used in the SEA analysis for the 1971-75 period. A more detailed description of the preparation of these data is given by Halliwell and Allen (1984). North of about 30°N these winds have proven to be useful and representative (Halliwell and Allen, 1984, 1987), but off southern Mexico and farther south their quality has

not been tested. We use them there for geographic completeness, but with reservations. For coastal locations in Peru and Ecuador we use synoptic meteorological data obtained from the respective navies of those countries. The surface wind observations at Talara and Callao have been used in other studies (Enfield, 1981a, 1981b) and we believe them to be representative of coastal winds along the Peru coast. The winds at Salinas are measured at an airport located on a narrow peninsula surrounded by open ocean. For Nauru we use the zonal wind component derived from a combination of the FNOC spot weather data (courtesy D. Luther)

TABLE 1. Given for each sea level station is its name, abbreviation, location, data source and distance along the equator and coast from Nauru Island, followed by the name and data source for the local surface wind station. Data sources are: University of Hawaii (UH), Instituto Oceanografico de la Armada del Ecuador (INOCAR), Direccion de Hidrografia y Navegacion de la Marina del Peru (DHNM), Corporacion de Aviacion Civil del Peru (CORPAC), Instituto Geografico Agustin Codazzi de Colombia (IGAC), Universidad Nacional de Costa Rica (UNCR), Universidad Nacional Autonoma de Mexico (UNAM), NOAA/National Ocean Survey (NOS) and the U.S. Navy Fleet Numerical Oceanographic Center (FNOC).

SLH station	Abbr.	Lat	Long	Dist (km)	Source	Wind station	Source
Nauru Is.	NAU	0°30'S	166°52'E	0	UH	Tarawa	UH
Christmas Is.	CHR	2°20'S	157°40'W	3 970	UH	(none)	(none)
Santa Cruz	STZ	0°45'S	90°19'W	11 460	UH	(none)	(none)
La Libertad	LLB	2°12'S	80°55'W	12 520	INOCAR	Salinas	INOCAR
Talara-Paita	TPA	4°37'S	81°17'W	12 790	DHNM	Talara	CORPAC
Callao	CAL	12°03'S	77°09'S	13 730	DHNM	Callao	CORPAC
Buenaventura	BVA	3°54'N	77°05'W	13 020	IGAC	SG-02	FNOC
Quepos	QPO	9°42'N	84°10'W	14 040	UNCR	SG-04	FNOC
Acapulco	ACA	16°51'N	99°55'W	16 050	UNAM	SG-11	FNOC
San Diego	SDO	32°43'N	117°10'W	18 610	NOS	CG01-02	FNOC
San Francisco	SFO	37°48'N	122°28'W	19 370	NOS	CG06-07	FNOC

from five closely grouped islands: Tarawa, Nauru, Ocean, Beru and Arorae (Table 1). The surface wind data available from locations near Christmas and Santa Cruz Islands were inadequate for analysis. All wind data were checked for outliers, filtered and decimated to daily values in a manner consistent with the treatment of the SLH data. Two short gaps in the daily filtered winds at Talara were filled with the autoregressive prediction filter.

Surface atmospheric pressure was available from the same sources as the surface winds, and was added to the SLH series to produce "adjusted" sea level at all stations except the three equatorial island locations. Because the adjusted SLH is thought to correspond more closely to subsurface pressure, it is the more dynamically relevant form of sea level. It has been consistently shown that the pressure correction for sea level becomes unimportant at very low latitudes (e.g., Enfield and Allen, 1980; Spillane et al., 1987). It can be seen from Table 2 that the rms amplitude of the pressure in the 40–60 day band—as compared with that of SLH—decreases equatorward, and that the coherence between adjusted and unadjusted SLH increases to very large values. Over a limited period for which Tarawa Island pressures were available (1983–85), the adjusted and unadjusted SLH at nearby Nauru have very similar autospectra and high coherence in the intraseasonal band (Table 2). Thus, in all of the analyses, the unadjusted SLH from the three equatorial stations are combined with the adjusted coastal data under the assumption that neglect of the pressure correction is unimportant.

Apart from the winds near the sea level stations (Table 1), we also use the zonal component of the surface winds measured by the EPOCS buoy at 110°W during 1980–82 (courtesy D. Halpern). For the critical far western Pacific, we obtained surface synoptic ship reports for the ten-degree square centered at 150°E on the equator, an area that straddles a heavily traveled

shipping lane from Japan to New Caledonia. Following the elimination of duplicate reports and outliers, we retrieved an average of six observations per day, with data densities that permitted vector averaging to daily values from October 1980 through December 1984. Among these we found 67 small gaps of one or two days, which we bridged by autoregressive prediction to complete the 53 month series.

The last major dataset used in this study consists of five-day averaged 850 mb wind fields on a five degree square grid for the world as far as 40°S (courtesy K. Weickmann). The data are not actual observations; they are the values output by the National Meteorological Center (NMC) model, which assimilates sounding data and cloud motion winds when and where they exist, using model output to "massage" the observations. At times and places where data are scarce, the "first guess" field from the model dynamics is used. In the equatorial Pacific, where the data coverage for low-level winds is good, the 850 mb wind product is mainly a model-massaged analysis that is weighted more heavily by sounding data in the western Pacific and by cloud motion winds in the central and eastern equatorial Pacific (Kousky, personal communication). Each year contains 73 five-day averages (pentads) except in leap years; the last day of February in leap years goes into a six-day average, which is treated with the same weight as pentads in the analyses. The only processing done on this data was to use the autoregressive prediction filter to fill three gaps in which entire fields were missing for one or two pentads. The 850 mb data were subsampled into two smaller Pacific grids: a basin scale grid with 102 points at ten-degree intervals staggered in latitude from 20°S to 40°N and 120°E to 70°W; and a 25-point one-dimensional grid over the equatorial and coastal waveguides (see Fig. 1). Whenever the 850 mb data are jointly analyzed with SLH or surface winds, the latter sets are first reduced to pentads for compatibility.

TABLE 2. Ratio of rms atmospheric surface pressure variation $\langle p \rangle$ to the rms (unadjusted) SLH $\langle h \rangle$, and coherence-squared between adjusted and unadjusted SLH; coherence-squared and lag of SLH with respect to the local surface wind; and coherence-squared and lag of SLH with respect to the local wind at 850 mb. Statistics are computed for the period mid-February 1980 through March 1984 for the 40–57 day band with 24 degrees of freedom. Values of coherence-squared of 0.19 are significant at the 90% confidence level. Positive lags imply that wind precedes SLH.

SLH station	Adj./unadj. SLH		Surface wind vs SLH		850-mb wind vs SLH	
	$\langle p \rangle / \langle h \rangle$	Coh. sq.	Coh. sq.	Lag (days)	Coh. sq.	Lag (days)
Nauru	0.171	0.96	0.30	+2.2	0.47	+4.6
Callao	0.168	0.96	0.02	-22.5	0.08	-20.2
Talara-Paita	0.226	0.96	0.08	+19.4	0.01	+19.6
La Libertad	0.141	0.98	0.07	-5.0	0.00	-3.2
Buenaventura	0.116	0.98	0.13	+8.7	0.03	-2.3
Quepos	0.116	0.99	0.13	-14.1	0.03	-17.9
Acapulco	0.152	0.99	0.23	-17.4	0.21	-15.8
San Diego	0.495	0.87	0.34	-4.3	0.25	+0.7
San Francisco	0.467	0.92	0.43	+2.9	0.51	+3.0

3. Descriptive characteristics of the data

Before showing the results of the statistical analyses, we wish to describe the spatial and temporal characteristics of the principal sea level and wind datasets. It is especially important to establish the 850 mb winds as being representative of the atmospheric intraseasonal oscillation described by others, prior to demonstrating its connection to the 40–50 day sea level signal.

a. Sea level

Figure 2 shows the 1979–84 time series of SLH at the 11 stations whose locations are given in Fig. 1 and Table 1. For clarity, the series are smoothed with a very-low-pass (VLP) filter having an amplitude response of 10%, 50% and 90% at periodicities of 23, 30 and 43 days. Obvious features in the data include a regular annual variation north of the equator, a relative lack of annual variability in the central and eastern equatorial and South Pacific, and high sea levels from mid-1982 through mid-1983, associated with the El Niño episode. More pertinent to this paper are the ubiquitous oscillations with periodicities of about 40–60 days. These are found during most of the six-year data period and have no obvious annual modulations in amplitude. Interannually, however, the oscillation appears to be especially regular during 1980–82, but decreases in amplitude in 1983–84, particularly evident at low latitudes during the recovery phase of the El Niño. Similar interannual modulations of amplitude are seen in the SEA analysis of the 1971–75 period, with a corresponding hiatus in 1973 during the recovery phase of the 1972–73 El Niño (Fig. 2 of SEA).

Important meridional variations in the amplitude of the 40–60 day signal can also be seen in Fig. 2. Referring to the eastern boundary region, note that amplitudes are small at Santa Cruz, on the equator, and increase poleward into both hemispheres to maximum values at Acapulco in the north and Callao in the south. Also, an abrupt decrease in amplitude occurs at the California stations. Both the interannual and meridional variations in amplitude mimic behavior seen by SEA in the 1971–75 dataset, and will be more fully described in later sections.

b. Winds

The dominant spatial structures of amplitude and phase for the winds are extracted for 1980–84 by performing an FDEOF analysis on the large scale gridded 850 mb wind data for the 40–57 day period band. This band was chosen because it best characterizes the frequency range of the large scale coherence found in SLH. The 102×102 element cross spectral input matrix was constructed by band-averaging 14 raw spectral estimates in the 40–57 day period range, resulting in 28 degrees of freedom for the band. The first, second and third eigenmodes explain 27%, 19% and 12% of

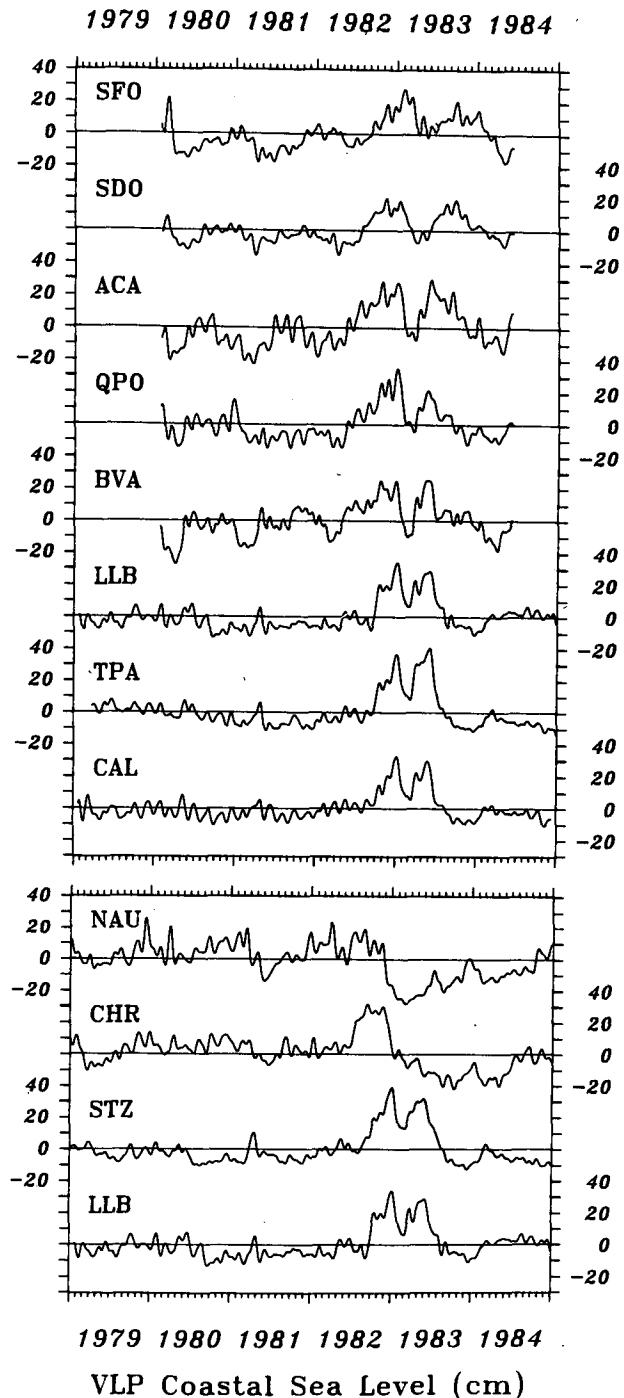


FIG. 2. Time series of sea level for 1979–84, with series means removed and smoothed with the very low pass (VLP) filter. Upper panel is for the meridional coastal array. Lower panel is for the zonal equatorial array, with La Libertad repeated from the upper panel. Station abbreviations are defined in Table 1 and refer to locations shown in Fig. 1.

the total variance in the data, respectively. According to the method outlined by Overland and Preisendorfer (1982) for testing the significance of eigenmodes, only

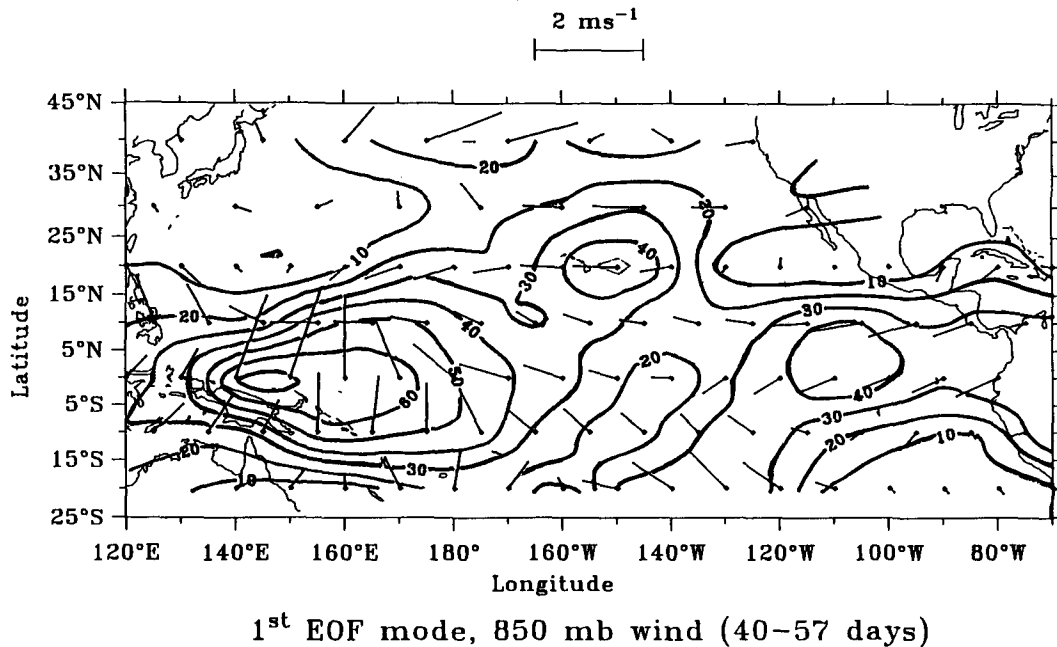


FIG. 3. First eigenmode of the frequency domain EOF of the large scale grid of 850 mb winds. Contours give the explained variance in percent. The scale at the top is for vector lengths, which are proportional to the rms amplitudes. Counterclockwise rotation of the vectors indicates advancing phase, completing the full circle in one 47-day period.

these first three modes are significant at the 95% level of confidence.

The distributions of explained variance, rms amplitude and spatial phases are shown in Fig. 3 for the first eigenmode. The explained variance (EV) is greatest (50%–70%) in the western Pacific between 10°S–10°N and 135°E–180°. A secondary EV maximum (>40%) occurs near 110°W, just north of the equator, and another over the Hawaiian Islands. A tertiary EV maximum (>20%) occurs in the westerly belt, north of 35°N. Along the eastern boundary, the signal strength is maximum from 5°S to 15°N (>30%); it falls off toward the poles but undergoes a secondary increase to 19% and 16% near Ensenada and San Francisco, respectively. The rms amplitudes in the tropics generally resemble the explained variance, being largest in the western Pacific. The disproportionately large amplitudes along 40°N are due to the very large total band energies that exist in the westerlies (see Fig. 1).

The dominant feature of the phase structure is a regular eastward propagation along the equator in the western Pacific. The phase is zonally uniform in the far western Pacific, advances regularly from 150°E to 170°W and again becomes zonally uniform farther east. The phase also remains approximately uniform along the eastern boundary from northern Peru to California. The region of regular phase propagation in the western equatorial Pacific coincides with the large area where the first mode signal is dominant. The fluctuations at 170°W lag those at 140°E by 12 days, yielding a phase speed of about 5 m s⁻¹. In contrast, the phase

advances from 170°W to South America by only an additional five days, resulting in an overall phase lag of 17 days and a zonally averaged speed of 10 m s⁻¹.

The similarity of the results shown in Fig. 3 to the analyses of others underlines the dominance and robustness of the oscillation, and clearly demonstrates that the first eigenmode shown here is a faithful representation of that process. For example, the extensive analyses of Lau and Chan (1985) and Weickmann et al. (1985) both show a region of most intense activity between Indonesia (120°E) and the dateline, with a regular eastward propagation of anomalies between these two regions. Weickmann et al. (1985) find a propagation of about 5 m s⁻¹ from the mid-Indian Ocean (west of the domain analyzed here) to at least 160°E, in agreement with the original results of Madden and Julian (1971, 1972). The study by Weickmann et al. (1985) also indicates a weaker, but significant oscillation in the eastern equatorial Pacific OLR, as well as phases that are relatively stationary there and lag the western Pacific by similar amounts to those found here for the 850 mb winds. As in Fig. 3, the studies of both Lau and Chan (1985) and Weickmann et al. (1985) find a region of secondary oscillation activity near the Hawaiian Islands, consistent with the 850 mb distributions shown here. Finally, a recent analysis by Knutson and Weickmann (1987) of the 850-mb wind oscillation also shows the uniform phase extending from the central equatorial Pacific northward to the Hawaiian Islands, and the reversal of phase in the central north Pacific (40°N).

The principal features of the second FDEOF (not shown) are two zonal bands of moderately large explained variance: one (30%–40%) is due west of Costa Rica along 10°N to 140°W, and the other (30%–50%) is north of 35°N and east of Japan to about 150°W. The highest EV along the equator is in the central Pacific (20%–30%) from 120° to 160°W. The third mode (not shown) has isolated points of higher EV centered at the Galapagos (37%) and San Francisco (55%). These features do not correspond to widely recognized characteristics in the global intraseasonal oscillation.

c. Wind vs sea level

Figure 4 shows the contoured time–longitude distribution of the zonal component of the 850 mb winds at ten degree intervals along the equator from 135°E to 85°W, and compares them to the VLP-filtered time series of the surface zonal wind index at 170°E, the alongshore component of the surface wind at Talara, Peru, and the adjusted SLH at Callao. The 850 mb winds reproduce many of the features known to exist in the surface winds along the equator, such as strong easterlies in the central Pacific, frequent westerlies in the western Pacific, and the large, eastward migrating perturbation from mid-1982 to mid-1983, associated with the El Niño/Southern Oscillation (ENSO) episode. Also seen are fairly regular intraseasonal oscillations with a very slight tilt indicating their rapid eastward propagation, consistent with the discussion of Fig. 3.

It is clear that the 850 mb winds are representative of much of the surface wind variability in the equatorial Pacific at time scales of a month or more, explaining many of the features found in the Peru coastal sea level. The time of most intense eastward winds at 170°E (November 1982) precedes the maximum peak in the Callao SLH by about 50 days. It was shown by Enfield and Lukas (1984) that when the 170°E winds are offset by 50 days, most of the prominent features, including the intraseasonal oscillations, are aligned with the corresponding facets of the SLH series at the Peru coast. This is the approximate time required for lowest baroclinic mode equatorial Kelvin waves to travel from 170°E to South America (Lukas et al., 1984). The only notable lack of visual correlation between Callao SLH and the 170°E surface wind occurs during the second period of high sea levels in the later (1983) phases of the El Niño. It has been shown by others (e.g., Philander and Siegel, 1985) that the relaxation of the winds off Ecuador produced high eastern Pacific sea levels in 1983. This can be readily seen in Fig. 4, where the weakening of the Talara wind and the arrival of 850 mb westerlies along the equator near 85°W coincide with the second peak in the Callao SLH.

Because 50 days is also the approximate periodicity of the intraseasonal oscillation in both the 170°E winds and the Callao SLH, there is a cyclical ambiguity between lags of zero or 50 days. It seems unlikely that

South American SLH could be directly associated with western Pacific winds at zero lag, but it might be associated with a zonally coherent trans-Pacific wind oscillation with small zonal phase changes. Fig. 3, however, shows that the wind oscillation requires at least two weeks to propagate from the western Pacific to the South American coast. This makes a zero phase relationship seem unlikely.

4. Autospectra

The autospectra from the 1980–82 period when the 40–50 day signal was well developed are shown in Fig. 5 for the sea level at Nauru and Callao, the 850 mb wind at 145°E, and the surface wind at 150°E, 170°E and Callao. Except for the surface wind at 170°E and Callao, the spectra have significant peaks centered near the 50 day period that constitute the dominant feature. The most impressive case is that of the Callao SLH, where the peak is best developed between 43 days and 65 days and stands an order of magnitude above the background. The peak in the surface wind at 150°E has less energy than that of the 850 mb wind at 145°E, as expected from frictional effects in the planetary boundary layer. The peak in the Callao wind is the least well defined and lies more than an order of magnitude lower than that of the surface wind at 150°E.

The distribution of spectral density as a function of time and frequency is contoured in Fig. 6 for the 850 mb wind at 145°E and the Callao SLH. The plot shows interannual variations but does not resolve annual or shorter period variability. Particularly evident during the three year period 1980–82 is a prominent ridge of high energy in sea level centered at frequencies of 0.021 to 0.017 cpd (48–57 days), with a nearly tenfold increase over background levels at higher and lower frequencies. Although the ridge–trough signature of the 40–60 day oscillation signal can be traced into 1979, it is definitely weaker during that year. The large increase in energy at very low frequencies, associated with the 1982–83 El Niño, coincides with the disappearance of the 40–60 day oscillation ridge in 1983. The high SLH energy near 0.05 cpd in early 1983 is part of a ridge of relatively high energy that extends toward higher frequencies during the time of the El Niño.

The time–frequency distribution of wind energy at 145°E is similar, with a ridge–trough structure in the oscillation band roughly like that of SLH. As with sea level, the ridge in wind energy weakens in late 1979, is well defined in 1980–82, and disappears in 1983. The period range is a bit lower for the ridge in winds—40–53 days as opposed to 48–57 days for SLH. The pattern of high SLH energy at low and high frequencies during 1983 (vertically oriented ridge) is not repeated in the wind. In fact, SLH energy is maximum in the 200–300 day band in early 1983, before the wind energy also becomes maximum. SLH energy is also maximum in the 20–25 day band during January–March 1983,

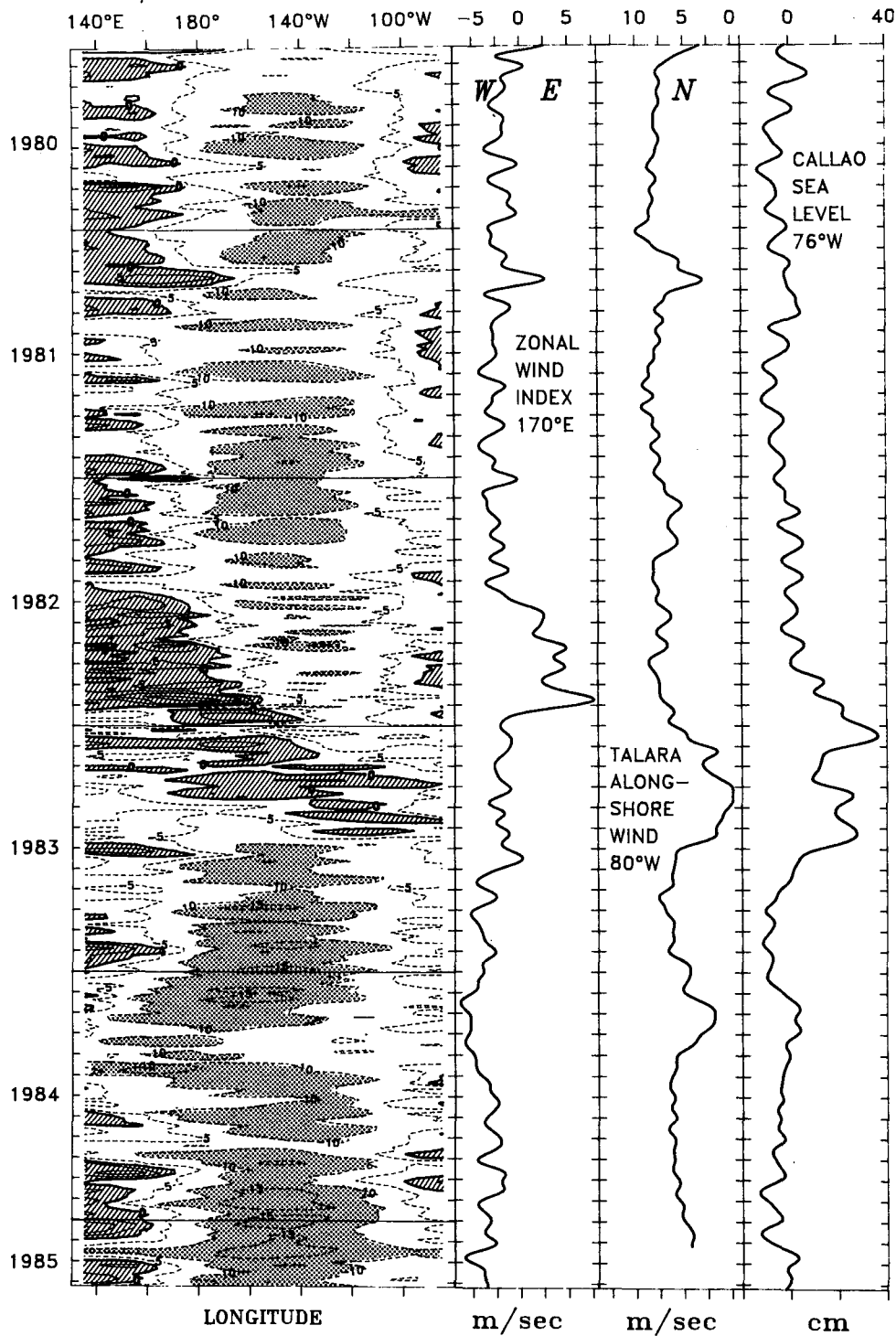


FIG. 4. From left to right, with time plotted downward: (a) time-longitude diagram of the 850 mb zonal wind speed along the equator; (b) the zonal surface wind on the equator near 170°E; (c) the northward (alongshore) component of the Talara wind (increasing to left); and (d) the adjusted Callao sea level. The 850 mb contour interval is 5 m s⁻¹, stippled shading indicates westward winds in excess of 10 m s⁻¹, and cross hatching indicates eastward winds.

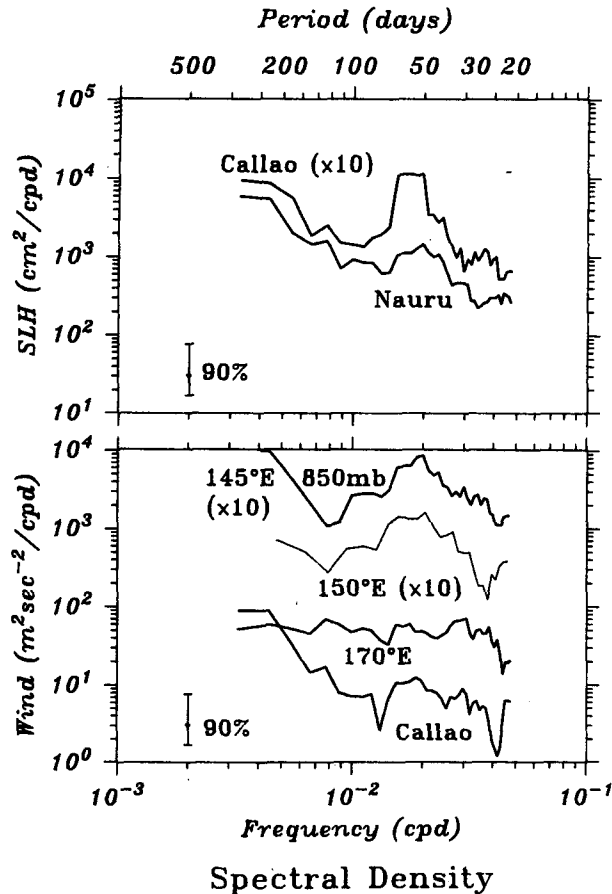


FIG. 5. From top to bottom, autospectra for selected sea level and equatorial wind series as follows: (upper panel) sea level at Callao and Nauru; (lower panel) 850 mb zonal wind at 145°E, and surface winds at 150°E, 170°E and Callao. Except for the 150°E surface wind, all calculations are for the period from January 1980 through June 1982, using running band averages with 10 degrees of freedom. The shorter series from 150°E covered the period from October 1980 through June 1982. For clarity, several spectra are plotted at one decade above their true value ($\times 10$).

at which time the corresponding wind energy is relatively low. Hence, only the intraseasonal oscillation shows a clear relationship between the two variables.

The lack of stationarity in the oscillation signal dictates caution in performing statistical analyses on the data. To avoid difficulty and explore interannual differences in oscillation characteristics, we have therefore split our computations into two periods of strong and weak oscillation: from January 1980 through June 1982 and from January 1982 through mid-1984, respectively. The differences between these two periods prove to be most significant along the equator.

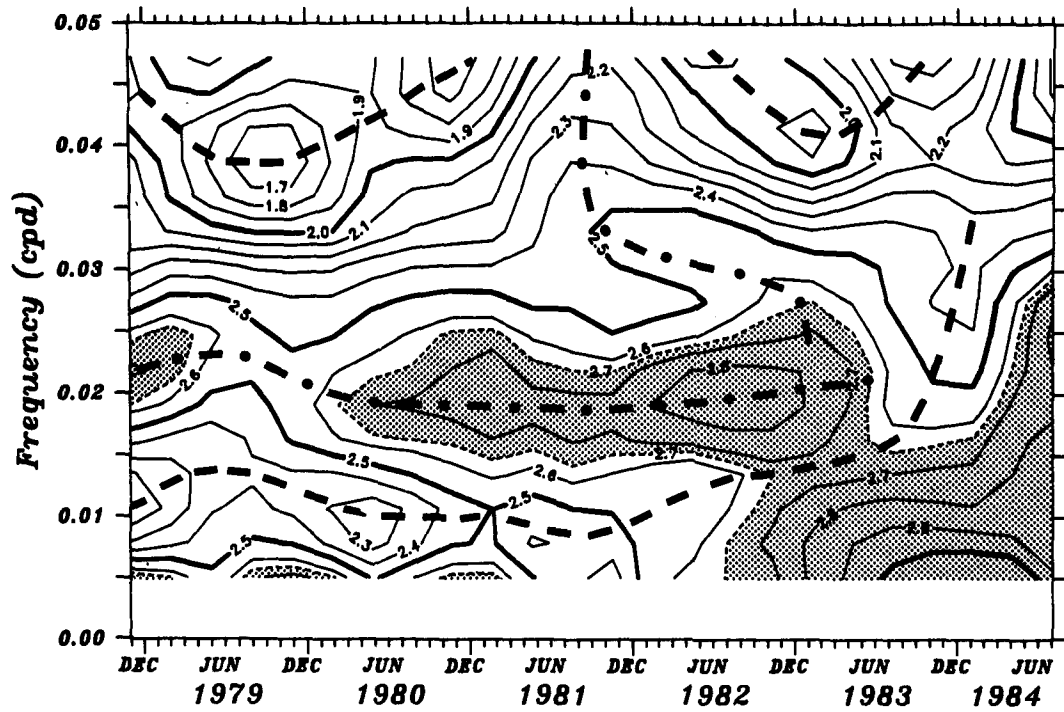
5. Local wind forcing

Table 2 lists the coherence-squared and phase lag for the 40–57 day band between the sea level and the local alongshore surface wind at each location shown

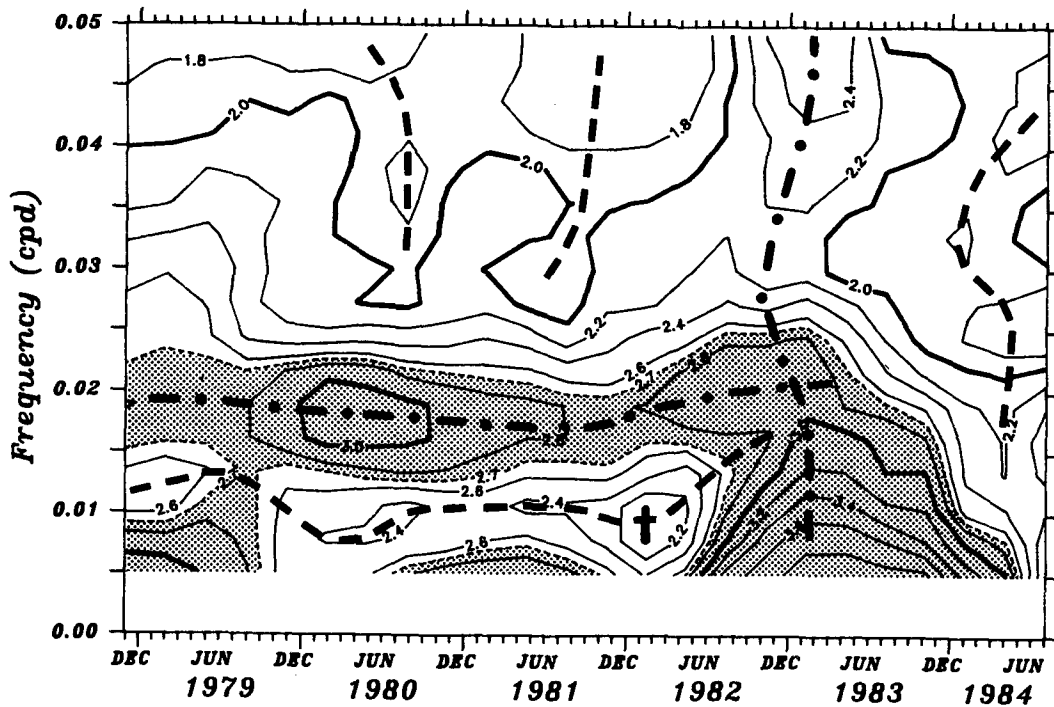
in Fig. 1, and also between the sea level and the low level wind at the nearest 850 mb grid point (the 40–57 day principal axis component shown in Fig. 1). The comparisons between SLH and the 850 mb winds confirm the surface results everywhere. At east Pacific stations south of Acapulco the wind is incoherent with sea level and the lags are not consistent with local forcing. Significant coherence at Nauru suggests that local or regional forcing is potentially important there. Significant coherence also occurs north of Quepos, but the lag at Acapulco is large.

The coupling between Nauru sea level and the western Pacific winds is probably stronger than indicated by the significant but low coherence between Nauru SLH and the 170°E surface wind (Table 2). The coherence spectrum between Nauru SLH and the 170°E surface wind is significant in the 30–50 day range, but not in the lower frequency portion of the 40–57 day band (Fig. 7). Similar instances of null or off-center coherence are observed between the 170°E wind and other sea level stations. In contrast, the coherence spectrum between the Nauru SLH and the zonal surface wind at 150°E shows very high coherence, well centered in the oscillation band (Fig. 7). A similar, strong spectrum was obtained between Nauru SLH and the zonal 850 mb wind at 145°E (not shown). Our results are generally consistent with Luther's (1980) finding that wind and sea level were related in the 35–80 day band at Canton Island (2.8°S, 173.7°W). They suggest, moreover, that the SLH oscillation at Nauru is more effectively forced by the winds over a considerable distance to the west than by the local winds.

The significant coherence at the California stations is probably misleading for two reasons: First, the wind energy and its coherence with SLH are maximum in period ranges to either side of the 40–57 day band (not shown). Second, less than 20% of the 40–57 day 850 mb wind variance at these locations is explained by the large scale pattern shown in Fig. 3 (first FDEOF mode). More of their variance is explained by the second eigenmode near San Diego (35%) and by the third eigenmode near San Francisco (55%). Breaker and Lewis (1988) find a relationship between California coastal ocean temperatures and local winds in a band centered near 47 days (1966–76), but not between sea level and winds. We also note that Knutson and Weickmann (1987) find some evidence for seasonally dependent teleconnections between the tropical oscillation and the region off the west coast of North America. Hence, although local winds appear to contribute to the intraseasonal band of California SLH, this forcing may be strongly intermittent and only weakly related to the atmospheric oscillation described in the meteorological literature for the global tropics. Conversely, and consistent with calculations done in the SEA analysis, we find that the 30%–45% of California SLH variability that is coherent with the large scale FDEOF of SLH (section 7) is incoherent with the local



Log of Spectral Density, 850mb Zonal Wind at 145°E



Log of Spectral Density, Callao Sea Level

FIG. 6. Contour plots of the log of spectral density as a function of time and frequency for the 850 mb zonal wind at 145°E (top) and the Callao sea level (bottom). Spectra are computed for yearly segments incremented by 90 days in time, with running band averages having six degrees of freedom. The chance probability that a feature lies more than 0.32 above a given value is less than 10%. Shading indicates log values above 2.7. Major troughs and ridges are highlighted with dashed and dot-dashed lines, respectively.

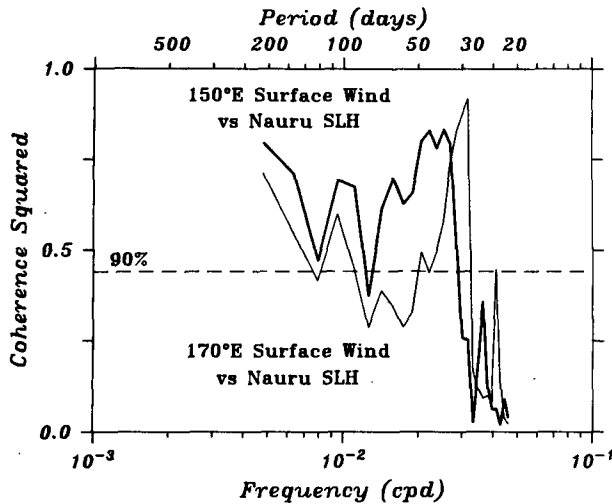


FIG. 7. Spectra of coherence-squared for equatorial winds at 150°E and 170°E vs the sea level at Nauru Island. Calculations are done for the period from October 1980 through June 1982, using running band averages with 10 degrees of freedom. The horizontal dashed line indicates the significance level at 90% confidence.

winds. We conclude, as SEA do, that the large scale oscillation signal in sea level is essentially unforced along the eastern boundary. Any forcing of SLH that does occur in California is, at best, only weakly related to the atmospheric oscillation in the tropics.

If the SLH oscillation is remotely forced in the western Pacific, one anticipates that the sea levels from the low latitude eastern boundary are also coherent with western Pacific winds, but at large lags. This can be seen for the high-frequency portion of the oscillation band in a figure from Eriksen et al. (1983), which shows a 40 day coherence peak between winds at Beru Island (1.3°S, 171.0°E) and a year-long pressure gauge record from Isabela Island (0.0°S, 91.5°W), at a lag of 43 days (their analysis did not resolve the low-frequency portion of the intraseasonal band). Also in agreement with this expectation, we find that the intraseasonal SLH variability at low latitude stations such as Callao and Talara is quite coherent with the zonal 850 mb winds at 145°E, with large phase lags that are consistent with an oceanic propagation from the western Pacific. The coherence and phase spectra (not shown) are similar to the ones shown for Nauru SLH versus Talara-Paita SLH (Fig. 8).

6. Sea level propagation

Direct evidence of the oceanic propagation of the sea level oscillation can be seen by comparing the SLH series with each other, as in Fig. 8. The sea levels at Talara and Callao have high coherence over a large range of frequencies, with a maximum in coherence-squared in the 40–57 day band and phases that indicate a rapid poleward propagation at about 5 m s⁻¹. When

SLH is compared between Nauru and Talara, the variability becomes incoherent or marginally coherent over most of the 0.003–0.050 cpd frequency range, but remains quite high in the 40–57 day band, with phases indicating an equatorial propagation of about 3 m s⁻¹. As pointed out in reference to Fig. 4, we see a cyclical ambiguity, or “phase wrap”, that occurs due to the large distance between Nauru and Talara. Fortunately, this spatial aliasing can be detected and overcome because meaningful phases occur even where the coherence is marginal or insignificant, so that a linear phase-frequency relationship emerges clearly. This relationship is consistent with the nondispersive nature of Kelvin wave propagation.

To characterize the propagation between stations, we calculated SLH phase speeds by three methods: one wide-band and two band-specific (Table 3). The wide-band procedure involves computing a weighted least-squares linear fit to each phase spectrum. The fitting

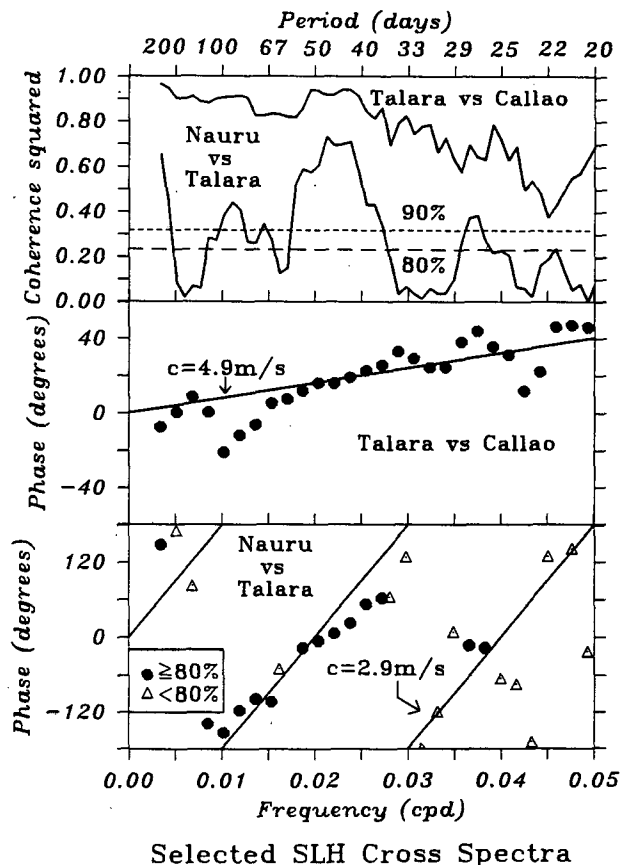


FIG. 8. Coherence and phase spectra for two pairs of sea level stations: Talara vs Callao and Talara vs Nauru. Calculations are for the period from October 1981 through December 1984, using running band averages with 12 degrees of freedom. Tilted lines on the phase spectra are the weighted least squares linear fits, constrained to pass through the origin. The weighting scheme is based on the estimates of coherence-squared and is explained in detail by Enfield and Allen (1983).

TABLE 3. Propagation statistics for the period January 1982 through June 1982, from left to right following the station identification and interstation distance: coherence squared and phase speed (m s^{-1}) between stations, based on cross spectrum in the 40–57 day band; coefficient of determination (R^2) and phase speed corresponding to a weighted least-squares linear fit of phase and frequency over the frequency range 0.003–0.050 cpd; and phase speed determined from the phase difference in the first FDEOF mode of the SLH array. For comparison, the column on the far right shows the FDEOF speeds for the January 1982 through April 1984 period. Phase speeds are all poleward, and the 90% significance level for coherence squared is 0.32. The upper and lower sections of the table refer to adjacent and nonadjacent station pairs, respectively.

Station pair	Dist. (km)	Statistics for 1980–82					1982–84	
		40–57 day band		Least-squares fit		FDEOF speed	FDEOF speed	
		Coh. sq.	Speed	R^2	Speed			
Adjacent								
NAU–CHR	3 970	0.43	3.1	0.99	2.8	2.9	2.8	
CHR–STZ	7 490	0.35	5.5	0.99	3.3	7.4	3.5	
STZ–LLB	1 060	0.56	1.4	0.56	3.6	1.7	7.9	
LLB–TPA	270	0.79	0.6	0.78	1.4	0.7	0.7	
TPA–CAL	940	0.86	21.8	0.58	6.4	24.7	5.3	
STZ–BVA	1 560	0.65	2.1	0.89	2.5	2.1	14.3	
BVA–QPO	1 020	0.81	2.6	0.86	2.0	2.6	1.8	
QPO–ACA	2 010	0.64	2.4	0.85	3.4	2.7	2.7	
ACA–SDO	2 560	0.46	2.0	0.96	2.1	1.7	2.1	
SDO–SFO	760	0.44	2.0	0.79	2.3	3.7	3.7	
Nonadjacent								
NAU–STZ	11 460	0.37	4.4	0.99	3.1	4.8	3.2	
CHR–LLB	8 550	0.17	4.7	0.99	3.3	5.2	3.8	
STZ–TPA	1 330	0.56	1.3	0.43	5.3	1.3	2.6	
LLB–CAL	1 210	0.83	2.9	0.66	4.4	2.7	2.2	
CHR–BVA	9 050	0.31	5.2	0.99	3.5	5.1	4.0	
STZ–QPO	2 580	0.47	2.2	0.91	1.8	2.3	3.8	
BVA–ACA	3 030	0.61	2.6	0.93	1.9	2.6	2.3	
QPO–SDO	4 570	0.61	2.0	0.97	2.0	2.0	2.3	
ACA–SFO	3 320	0.52	2.0	0.96	1.9	1.9	2.3	

procedure uses the Enfield and Allen (1983) weighting scheme based on the corresponding estimates of coherence squared. The resulting phase speeds are more stable than those determined from individual phase values and characterize the approximately nondispersive propagation that tends to occur over a wide range of periods (20–300 days), as in Fig. 8. The second method consists simply of computing the phase speed as the ratio of the interstation distance to the phase lag determined from the corresponding cross spectrum and averaged over the 40–57 day band. The third method consists of computing the speeds based on phase differences between stations in the first FDEOF eigenmode for the 40–57 day period band (section 7). The two band-specific methods give similar results except at the California stations, where the FDEOF explains less than 60% of the variability in the SLH data.

Except for the widely separated Christmas and La Libertad locations, the coherence between stations in the 40–57 day band is significant everywhere. The speed estimates become increasingly sensitive to uncertainties in the phase lags as the station separation decreases. For example, we find a lag of about two days between Talara-Paita and Callao for most choices of time period, which yields a southward propagation along the Peru coast of about 5 m s^{-1} (see Fig. 8 or the last column

of Table 3). For the 1980–82 period, however, the lag was only 0.5 days, resulting in a speed of 25 m s^{-1} (Table 3). Since a 1–2 day variation in lag is probably not significant, the two seemingly different speeds are effectively indistinguishable. When separations are increased by taking non-adjacent pairs, the speeds become less variable (Table 3, bottom).

In 1980–82, the linear-fit phase speeds in the 40–57 day band are about 3–7 m s^{-1} along the equator between Nauru and the Galapagos, while the wide-band estimate is close to 3 m s^{-1} . In 1982–84, the band-specific and wide-band estimates are all near 3 m s^{-1} (only the FDEOF values are shown in Table 3). During both periods, then, the equatorial propagation over most of the spectrum is consistent with the previous estimates of others (Knox and Halpern, 1982; Eriksen et al., 1983; Lukas et al., 1984). In the intraseasonal band, however, the equatorial propagation tends to be faster than at other frequencies, especially in 1980–82. The possible significance of this is discussed later.

Along the coast, the speeds are fastest at low latitudes ($2\text{--}5 \text{ m s}^{-1}$) and somewhat slower as the latitude increases into the Northern Hemisphere ($2\text{--}3 \text{ m s}^{-1}$). This behavior, which is consistent with the results of SEA for 1971–75, does not seem to depend strongly on the time period chosen for analysis. Note that the sea level

propagation is not consistent with the phase structure seen in the large-scale wind field (section 3b, Fig. 3).

7. Frequency domain EOF analysis

Although the bivariate comparisons between key time series provide considerable insight, they do not take full advantage of the spatially distributed information available in the wind and SLH data fields. The band energy in any particular time series contains background variability that is part of the spectral continuum, as well as the spatially coherent oscillation signal of interest here. Moreover, as in the case of San Diego and San Francisco (section 5), certain subregions may contain forced signals in or near the oscillation band that are unrelated (or only weakly related) to the large scale processes of principal interest.

By using frequency domain EOF analyses, we eliminate the complicating effects of these secondary signals and focus exclusively on the spatially organized signals. FDEOF analyses were done separately for the two apparently different time periods discussed in relation to Fig. 6 (section 4): 1980–82, when the oscillation signals in both the atmosphere and the ocean were strong and 1982–84, when the signals were weak. The periods analyzed are about 2½ years long and overlap each other by six months. The 40–57 day band is chosen because it best represents the frequency range of large scale coherence found in the sea level array, and because the use of a wider band (such as would be more representative of the atmospheric process) involves computational problems for the cross-spectral analyses used as input for the FDEOFs (phase information becomes increasingly distorted). We applied the FDEOF analysis separately to the 11-point array of SLH stations and to a 21-grid point array of the 850 mb wind grid that overlies the equatorial and coastal waveguides south of 20°N (Fig. 1). The 850 mb winds are used in preference to the surface winds primarily because the latter are available for only two locations along the equator, but also because the FNOC winds (Table 1) are of doubtful quality at low latitudes. Although the winds and sea levels are analyzed separately, both the coastal and equatorial points were included in each analysis. To simplify the presentations, however, the amplitudes and phases from all analyses are discussed jointly, first for the equatorial region and then for the coast (Figs. 9, 10).

The first three FDEOF components in the 1980–82 analyses explained 72%, 16% and 7% of the total variance in the winds, and 65%, 25% and 5% of the SLH variance; the corresponding values for the 1982–84 period are 55%, 21% and 15% for winds and 69%, 14% and 10% for sea level. By the eigenmode selection rules of Overland and Preisendorfer (1982), the second and higher SLH modes are insignificant at the 95% confidence level and the second wind modes are marginally significant. Only the first FDEOF modes are shown

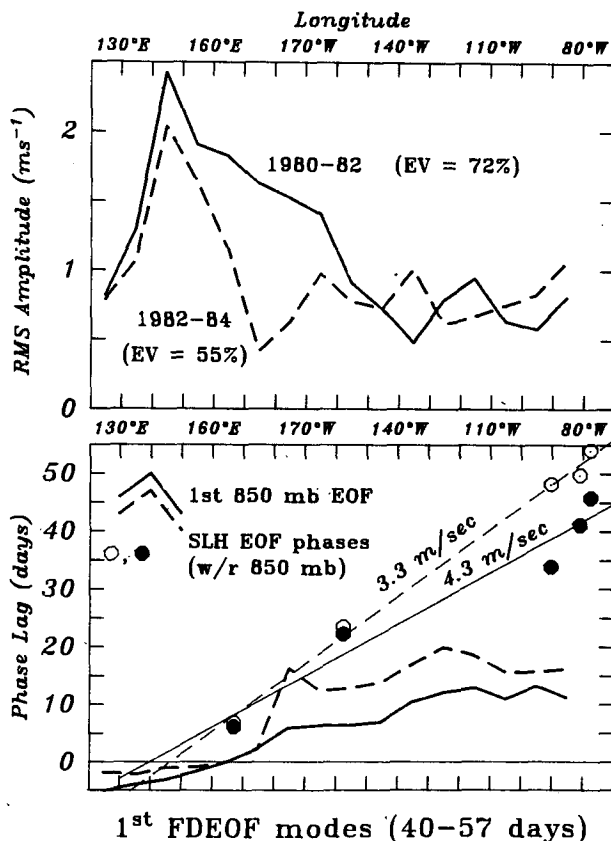


FIG. 9. The first eigenmodes of the frequency domain EOFs of sea level and 850 mb winds (40–57 day band) at equatorial locations during two time periods: January 1980 through June 1982 (solid) and January 1982 through April 1984 (dashed). Upper panel: distribution of the rms amplitudes of the 850 mb zonal wind. Lower panel: phase lags for same, relative to zero phase at 165°E, plus the phase lags for the equatorial sea level stations from the FDEOF of sea level. The sea level phases are referenced to the lag of Nauru sea level with respect to the wind at 165°E. Tilted straight lines are the least-squares linear fits to the sea-level phase lags.

here, which appear to capture the important large scale intraseasonal variability in both the atmosphere and the ocean. The wind phase is arbitrarily chosen to be zero at 165°E, and the SLH phase (initially) to be zero at Nauru (167°E). The SLH phases were then adjusted by adding the phase between the two FDEOFs (Nauru SLH lagged the 165°E winds by 6–7 days during both time periods).

The most noteworthy features of the wind distributions for the two time periods (Fig. 9) are the large amplitude of the oscillation signal in the western Pacific and the rapid phase propagation along the equator, which can also be seen in the large scale 1980–84 analysis of Fig. 3 and in the results of previous meteorological studies. In 1980–82 the rms amplitude at 145°E is nearly 2.5 m s⁻¹ as compared with 0.5–1.0 m s⁻¹ east of 160°W, giving an order of magnitude difference in variance. The variance in 1982–84 is also maximum near 145°E but has a smaller magnitude in the entire

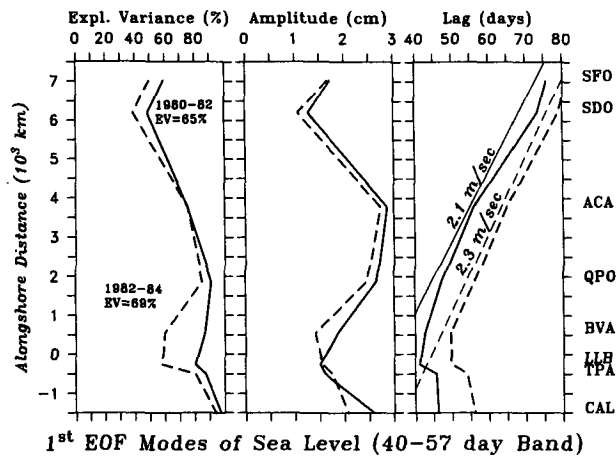


FIG. 10. The first eigenmodes of the frequency domain EOFs of sea level (40–57 day band) at coastal stations during two time periods: January 1980 through June 1982 (solid) and January 1982 through April 1984 (dashed). The meridional structure functions are shown (from left to right) for explained variance, rms amplitude and phase lag. Ordinates give the alongshore distance of stations from the equator (dashed line) in increments of 1000 km. Phases are referenced to the FDEOF of the 850 mb wind at 165°E, as explained in the text.

region between there and the Line Islands (160°W). In both periods the phase propagation of winds is slowest near the dateline (about 5 m s^{-1}) and fastest in the central and eastern Pacific ($15\text{--}20 \text{ m s}^{-1}$). The average phase propagation from 130°E to 80°W is $12\text{--}14 \text{ m s}^{-1}$ in 1980–82 as compared with $8\text{--}10 \text{ m s}^{-1}$ in 1982–84.

The SLH propagation along the equator was clearly faster in 1980–82 when the wind forcing was more intense and zonally extensive. Curiously, however, most of the speed increase occurred east of Christmas Island, rather than in the western Pacific where the wind oscillation is most energetic. Because the entire cluster of three eastern Pacific tide stations is shifted to smaller phase lags during this period, we are disinclined to suspect data peculiarities. Even if the Christmas Island data were faulty, the overall propagation east of Nauru would have been faster. We therefore conclude that an increase in the propagation speed of the intraseasonal SLH signal probably did occur and was confined mainly to the central and eastern Pacific. We will pursue this point further in section 8.

The distribution of SLH amplitude and phase along the eastern boundary (Fig. 10) is unaffected by the period chosen and corresponds closely to the findings of SEA for the 1971–75 period, as well as to our own bivariate statistics (Table 3). The rms amplitudes of the SLH signal increase by a factor of two from the equator to Acapulco and fall by a similar amount at stations north of the Gulf of California. It was shown by SEA that these features are consistent, respectively, with the conservation of energy density in frictionless, coastally trapped Kelvin waves within 20 degrees of

the equator, and with partial dissipation of the wave energy in the Gulf of California. The fact that propagation speeds along the coast are larger at low latitudes—also seen in Table 3 and the SEA analysis—is consistent with the behavior of low frequency coastal Kelvin waves (Cane and Sarachik, 1977). A linear least-squares fit to the SLH phases from Buenaventura to San Diego gives a poleward propagation of $2.1\text{--}2.3 \text{ m s}^{-1}$. This value is near the high end of the estimates found in the SEA analysis for the 1971–75 period.

8. Central Pacific forcing

The bivariate comparisons between SLH and local winds (section 5) clearly indicate that forcing occurs in the western Pacific and not along the eastern boundary. However, the rapid SLH propagation in the central and eastern equatorial zone during 1980–82 suggests that forcing may also be important there. In this section we present evidence to support this.

During 1980–82 the second FDEOF mode of the 850 mb winds (section 7) is most important in the central Pacific between 160° and 130°W, explaining 50%–51% of the total variability there as opposed to the 37%–43% explained by the first mode. Elsewhere, the second mode explains only 21%–25% (three grid points) or less than 15% (all other locations). Overall, the second mode explains only 16% of the wind variance, but is marginally significant. Surprisingly, however, when the first FDEOF mode of sea level is compared with the two wind modes, we obtain a coherence-squared that is actually higher for the second mode (0.57) than for the first mode (0.27). The second mode of the 850 mb wind was less important in 1982–84, explaining only 24%–33% of the total variance in the 130°–160°W longitude zone. Since the first wind mode was also weaker in 1982–84 and more confined to the western Pacific (Fig. 9), the weaker SLH oscillation and slower SLH propagation at that time are consistent with the relationships we see in 1980–82.

Although we lack surface wind data in the central Pacific, it is probable that the wind oscillation at the surface is significant there. Fig. 11 shows the autospectra and coherence spectrum of the 850 mb wind at 110°W and the surface wind measured by the EPOCS meteorological buoy at the same longitude, for the 1980–82 time period. We lacked the continuous buoy data needed to do similar computations for 1982–84. Both the wind series are an order of magnitude less energetic than their western Pacific counterparts, but have significant energy peaks in the intraseasonal band. The intraseasonal coherence between the surface and 850 mb is significant at the 90% confidence level and nearly reaches the 50% noise level. Thus, the intraseasonal signal in the winds at 110°W was comparatively weak but clearly present at both levels during the pre-El Niño time frame.

The effect of the central Pacific forcing can be seen rather dramatically in the coherence spectra between

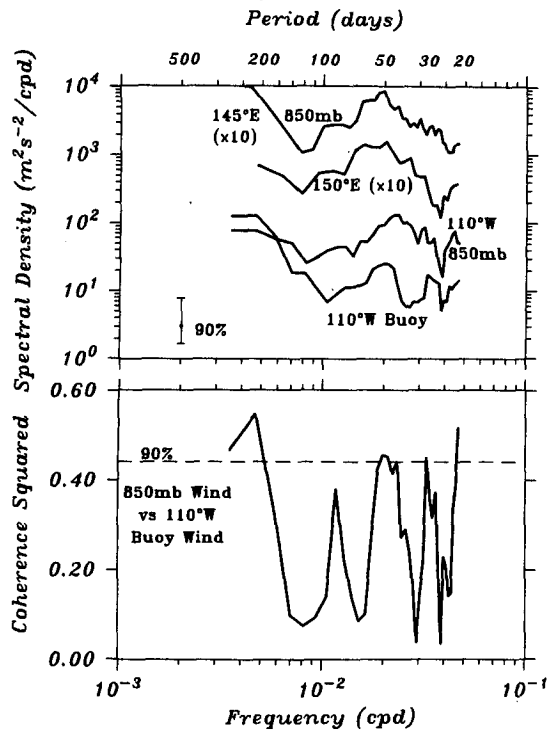


FIG. 11. Upper panel: autospectra of the 850 mb wind at 145°E and surface wind at 150°E, repeated from Fig. 5, plus the 850 mb wind at 110°W and the surface wind from the meteorological buoy at 110°W. Lower panel: spectrum of coherence squared between the 850 mb wind at 110°W and the surface wind from the meteorological buoy at 110°W. Calculations for the latter two series are done for the period from August 1980 through December 1982, using running band averages with 10 degrees of freedom. The horizontal dashed line indicates the significance level for 90% confidence.

equatorial tide stations (Fig. 12). From Nauru to Christmas Island the fluctuations at all periodicities below 25 days propagate eastward nondispersively at 2.8 m s^{-1} , as shown by the linear phase-frequency relationship. A similar, somewhat faster speed of 3.1 m s^{-1} occurs from Christmas to Santa Cruz at frequencies outside the intraseasonal band. However, a notable phase deficit occurs at the oscillation frequencies, indicating propagation of nearly 5 m s^{-1} there. These results were reflected, of course, in the statistics of Table 3.

In summary, the large scale SLH signal that reaches the eastern boundary appears to have been strongly modified by the central Pacific wind variability in 1980–82. This conclusion is tentative, however, due to the lack of surface wind data in that region.

9. Summary and concluding remarks

Over the 1980–84 period there existed a 40–60 day oscillation in eastern Pacific sea levels from Callao, Peru to San Francisco, California. The oscillation was best developed during 1980–82, with a central fre-

quency of 50–57 days and band limits of about 43–65 days. The large-scale coherence in sea level, however, was shifted somewhat toward shorter periods (40–57 days) than the maximum variance. The energy of the corresponding oscillation in the wind field occupied a similar period band as for sea level variance and displayed a large scale structure of amplitude and phase consistent with other descriptions of the intraseasonal oscillation in the atmosphere, being best developed in the western equatorial Pacific. Similar, interannual modulations of the oscillation amplitude occurred both in the western Pacific zonal winds and in sea level.

The most characteristic features of the SLH phase distributions along the equator are the regular patterns of eastward propagation and the near coincidence of wind and SLH phases west of the dateline, in a region where the wind variability is quite strong (section 7). Together with the bivariate analyses of sections 5 and 6, these results provide strong evidence that the intraseasonal oscillation in sea level analyzed by Spillane et al. (1987) is indeed forced in the western equatorial Pacific by the counterpart oscillation in the atmosphere.

The ocean-atmosphere coupling in the intraseasonal band is not confined solely to the western equatorial Pacific, where the wind variability is strongest, with essentially free wave propagation in the ocean between the dateline and South America. The intraseasonal

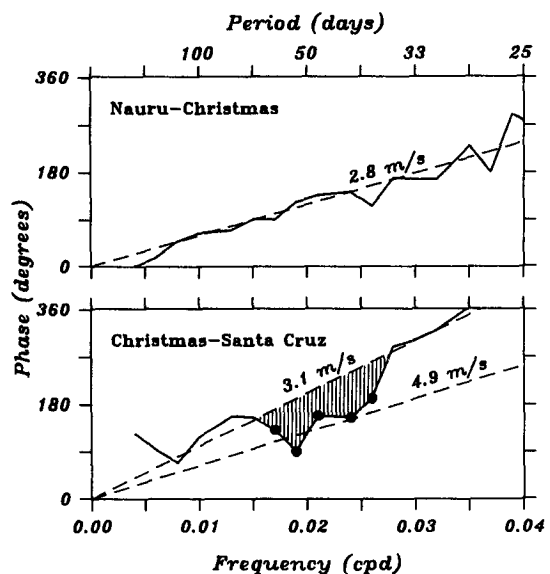


FIG. 12. Sea level phase spectra between equatorial Pacific islands. Calculations are done for the period from January 1980 through June 1982, using running band averages with 10 degrees of freedom. Weighted least-squares fits are indicated by the straight, dashed lines. Upper panel: Nauru to Christmas Island, with the propagation speed based on the fit to all phases shown. Lower panel: Christmas to Santa Cruz Island, with the faster propagation speed based on the fit to the intraseasonal phases only (solid circles). The lower speed is based on the fit to all other phases shown. The shading indicates the phase deficit in the intraseasonal band, discussed in the text.

band of equatorial sea level has unique characteristics as compared with other portions of the spectrum. Previous studies, e.g., of individual low-frequency events (Knox and Halpern, 1982), of the 1–6 week period range (Eriksen et al., 1983) and of wide-band phenomena in general, including El Niño (Lukas et al., 1984) have found propagation at speeds of 2.5–3.0 m s⁻¹ that is known (or presumed) to be forced in the western Pacific. Those results are consistent with the free propagation of lowest baroclinic mode Kelvin waves away from a remote region of stationary wind forcing. They are also consistent with the frequencies outside the intraseasonal band, in our own data. Within the intraseasonal band, however, we find much faster propagation of SLH phase in the central and eastern Pacific during 1980–82. At that time the atmospheric oscillation was more intense, extended more strongly into the central Pacific and also propagated faster. In contrast, during the 1982–84 period the oscillations in both winds and SLH were weak and almost disappeared during the mature and recovery phases of the El Niño. The strongest wind variance was confined to the western Pacific and the eastward propagation speeds of SLH were about 50% smaller between Christmas and Santa Cruz. The SLH propagation during this period was not very different from that observed previously by others and suggests that the fluctuations traveled as free waves over most of the equatorial waveguide and were predominantly forced in the western Pacific.

There is good coherence and continuity of phase between the sea level signal along the equator and its extension along the eastern boundary. Poleward phase speeds along the coast are rapid within about 5–10 degrees of the equator, consistent with theory. North of Buenaventura the fluctuations continued poleward at 2.1–2.3 m s⁻¹, consistent with freely propagating coastal trapped waves of lowest baroclinic mode. The meridional structure of FDEOF amplitude and phase in 1980–84 was very similar to that found in the analysis by Spillane et al. (1987) for 1971–75. The data also reproduce their finding that the oscillation has interannual modulations but no apparent seasonal variations in amplitude. Both datasets contain important El Niño episodes (1972–73 and 1982–83) and both studies find that the sea level oscillation is weakened or disappears during the year immediately following the El Niño.

The extensive meridional scale of the propagation along the eastern boundary is also significant. Large alongshore coherence scales have also been observed at interannual periodicities related to El Niño/Southern Oscillation (Enfield and Allen, 1980). Fluctuations at periodicities of a few days to several weeks having properties of coastal-trapped waves have been observed at various latitudes along the eastern boundary (Wang and Mooers, 1976; Brink, 1982; Enfield and Allen, 1983; Yao et al., 1984). Interestingly, however, the coherence scales are limited to 1000–2000 km, in spite of the fact that the offshore radiation of energy in the

form of long Rossby waves is not possible at such frequencies. The robust propagation properties of the low frequencies suggested by Spillane et al. (1987) and the present analysis seem to imply smaller dissipation rates. Finally, the large coastal coherence scale of the intraseasonal SLH signal lends credence to the suggestion that ENSO variability can propagate oceanically to midlatitudes (Enfield and Allen, 1980; Chelton and Davis, 1982), where it may become superimposed on variability forced locally or regionally (Simpson, 1983; Mysak, 1986). Indeed, both our analysis and the work of Breaker and Lewis (1988) suggests that a superposition of remote and local effects also occurs along the California coast in the intraseasonal band.

Our results raise a number of interesting questions whose final resolution is beyond the scope of this paper. Does the SLH signal that is generated in the western Pacific arrive essentially intact at the eastern boundary, or does significant energy loss occur, e.g., by beam propagation to the deeper ocean as suggested by McCreary (1984) and Rothstein et al. (1985)? The high coherence between SLH at Nauru and Talara (Fig. 8) suggests that the western Pacific variability survives, but in some years is “reworked” by the central Pacific winds. In other words, the propagating energy is probably confined to the near surface layer through the effects of vertical current shears or pycnocline reflections, as argued by McPhaden et al. (1986) and Gent and Luyten (1985), respectively. We will most likely answer these questions when realistic models separately trace the free and forced components of the variability along the waveguide, but this must await surface winds with better temporal and zonal resolution.

The last, and most tantalizing question is: Are the observed interannual differences in the wind forcing and ocean response related to ENSO cycles, and if so, in what way? The decrease in oscillation activity observed simultaneously in winds and SLH during the mature phase of the 1982–83 El Niño suggests this (Fig. 6) and is supported by a similar decrease in the SLH oscillation during the mature phase of the 1972–73 El Niño (Spillane et al., 1987). The possible importance of interannual variations and ENSO connections has already been suggested by atmospheric studies (Lau, 1985; Murakami et al., 1986; Lau and Chan, 1986). Eastward migration of atmospheric convective centers and the occurrence of ocean feedback to the atmosphere are important processes during ENSO episodes. How are such factors related to the suppression of the wind and SLH oscillations after ENSO anomalies have been well established?

Acknowledgments. I wish to acknowledge the helpful discussions of this research provided by my colleagues, Drs. R. Lukas, J. C. McCreary, J. S. Allen, M. C. Spillane and M. J. McPhaden. I am especially indebted to Dr. R. Lukas for his thoughtful comments on the manuscript. I also thank M. C. Spillane, P. M. Newberger, H. Pittock and M. P. Cornejo for their assistance

in processing and analyzing the data. I want to acknowledge and thank the organizations in North, Central and South America, cited in Table 1, that provided the coastal tide and meteorological data for this research, the University of Hawaii (Drs. K. Wyrski, R. Lukas and J. Sadler) for providing equatorial sea level and surface meteorological data, Dr. Klaus Weickmann for providing the 850 mb wind data, and the NOAA Environmental Research Laboratory (Mr. S. Woodruff) for providing ship-reported wind data. This research has been supported by National Science Foundation Grant OCE-8317390 and National Oceanic and Atmospheric Administration Grant NA85AA-D-CA024.

REFERENCES

- Anderson, J. R., D. E. Stevens and P. R. Julian, 1984: Temporal variations of the tropical 40–50 day oscillation. *Mon. Wea. Rev.*, **112**, 2431–2438.
- Breaker, L. C., and P. A. W. Lewis, 1988: A 40 to 50 day oscillation in sea surface temperature along the California coast. *Estuar. Coastal Shelf Sci.*, in press.
- Brink, K. H., 1982: A comparison of long coastal trapped wave theory with observations off Peru. *J. Phys. Oceanogr.*, **12**, 897–913.
- Cane, M. A., and E. S. Sarachik, 1977: Forced baroclinic ocean motions: II. The linear equatorial bounded case. *J. Mar. Res.*, **35**, 395–432.
- Chang, C. P., 1977: Viscous internal gravity waves and low-frequency oscillations in the tropics. *J. Atmos. Sci.*, **24**, 901–910.
- Chelton, D. B., and R. E. Davis, 1982: Monthly mean sea level variability along the west coast of North America. *J. Phys. Oceanogr.*, **12**, 757–784.
- Enfield, D. B., 1981a: Thermally driven wind variability in the planetary boundary layer above Lima, Peru. *J. Geophys. Res.*, **86**, 2005–2016.
- , 1981b: Annual and nonseasonal variability of monthly low-level wind fields over the southeastern tropical Pacific. *Mon. Wea. Rev.*, **109**, 2177–2190.
- , and J. S. Allen, 1980: On the structure and dynamics of monthly mean sea level anomalies along the Pacific coast of North and South America. *J. Phys. Oceanogr.*, **10**, 557–578.
- , and —, 1983: The generation and propagation of sea level variability along the Pacific coast of Mexico. *J. Phys. Oceanogr.*, **13**, 1012–1033.
- , and R. B. Lukas, 1984: Low-frequency sea level variability along the South American coast in 1982–83. *Trop. Ocean-Atmos. Newsl.*, **28**, 2–4.
- Eriksen, C. C., M. B. Blumenthal, S. P. Hayes and P. Ripa, 1983: Wind-generated equatorial Kelvin waves observed across the Pacific Ocean. *J. Phys. Oceanogr.*, **13**, 1622–1640.
- Gent, P. R., and J. R. Luyten, 1985: How much energy propagates vertically in the equatorial oceans? *J. Phys. Oceanogr.*, **15**, 997–1007.
- Halliwell, G. R., and J. S. Allen, 1984: Large scale sea level response to atmospheric forcing along the west coast of North America. *J. Phys. Oceanogr.*, **14**, 864–886.
- , and —, 1987: The large-scale coastal wind field along the west coast of North America, 1981–82. *J. Geophys. Res.*, **92**, 1861–1884.
- Knox, R. A., and D. Halpern, 1982: Long range Kelvin wave propagation of transport variations in Pacific Ocean equatorial currents. *J. Mar. Res.*, **40**(Suppl), 329–339.
- Knutson, T. R., and K. M. Weickmann, 1987: 30–60 day atmospheric oscillations: composite life cycles of convection and circulation anomalies. *Mon. Wea. Rev.*, **115**, 1407–1436.
- Lau, K. M., 1985: Subseasonal scale oscillation, bimodal climatic state and the El Niño/Southern Oscillation. *Coupled Ocean-Atmosphere Models*, J. C. J. Nihoul, Ed., Elsevier, 29–40.
- , and P. H. Chan, 1985: Aspects of the 40–50 day oscillation during the northern winter as inferred from outgoing longwave radiation. *Mon. Wea. Rev.*, **113**, 1889–1909.
- , and L. Peng, 1987: Origin of low frequency (intraseasonal) oscillations in the tropical atmosphere. *J. Atmos. Sci.*, **44**, 950–972.
- , and P. H. Chan, 1986: The 40–50 day oscillation and the El Niño: A new perspective. *Bull. Amer. Meteor. Soc.*, **67**, 533–534.
- Lukas, R., S. P. Hayes and K. Wyrski, 1984: Equatorial sea level response during the 1982–1983 El Niño. *J. Geophys. Res.*, **89**, 10425–10430.
- Luther, D. S., 1980: Observations of long period waves in the tropical oceans and atmosphere. Ph.D. thesis, Massachusetts Institute of Technology, 210 pp.
- McCreary, J. P., 1984: Equatorial beams. *J. Mar. Res.*, **42**, 395–430.
- McPhaden, M. J., J. A. Proehl and L. M. Rothstein, 1986: The interaction of equatorial Kelvin waves with realistically sheared zonal currents. *J. Phys. Oceanogr.*, **16**, 1499–1515.
- Madden, R. A., and P. R. Julian, 1971: Detection of a 40–50 day oscillation in the zonal wind field in the tropical Pacific. *J. Atmos. Sci.*, **28**, 702–708.
- , and —, 1972: Description of global scale circulation cells in the tropics with a 40–50 day period. *J. Atmos. Sci.*, **29**, 1109–1123.
- Mertz, G. J., and L. A. Mysak, 1984: Evidence for a 40–60 day oscillation over the western Indian Ocean during 1976 and 1979. *Mon. Wea. Rev.*, **112**, 384–386.
- Murakami, T., L. X. Chen, A. Xie and M. L. Shrestha, 1986: Eastward propagation of 30–60 day perturbations as revealed from outgoing longwave radiation data. *J. Atmos. Sci.*, **10**, 961–971.
- Mysak, L. A., 1986: El Niño, interannual variability and fisheries in the northeast Pacific Ocean. *Can. J. Fish. Ag. Res.*, **43**, 464–497.
- , and G. J. Mertz, 1984: A 40–60-day oscillation in the source region of the Somali Current during 1976. *J. Geophys. Res.*, **89**, 711–715.
- Overland, J. E., and R. W. Preisendorfer, 1982: A significance test for principal components applied to a cyclone climatology. *Mon. Wea. Rev.*, **110**, 1–4.
- Parker, D. E., 1973: Equatorial Kelvin waves at 100 millibars. *Quart. J. Roy. Meteor. Soc.*, **99**, 116–129.
- Philander, S. G. H., and A. D. Siegel, 1985: *Coupled Ocean-Atmosphere Models*, J. C. J. Nihoul, Ed., Elsevier, 517–541.
- Picaut, J., and J. M. Verstraete, 1976: Mise en évidence d'une onde de 40–50 jours de période sur les côtes de Golfe de Guinée. *Cah. O.R.S.T.O.M., ser. Oceanogr.*, **14**, 3–14.
- Rothstein, L. M., D. W. Moore and J. P. McCreary, 1985: Interior reflections of a periodically forced equatorial Kelvin wave. *J. Phys. Oceanogr.*, **15**, 985–996.
- Simpson, J. J., 1983: Large-scale thermal anomalies in the California Current during the 1982–83 El Niño. *Geophys. Res. Lett.*, **10**, 937–940.
- Spillane, M. C., D. B. Enfield and J. S. Allen, 1987: Intra-seasonal oscillations in sea level along the west coast of the Americas. *J. Phys. Oceanogr.*, **17**, 313–325.
- Wang, D. P., and C. N. K. Mooers, 1976: Long coastal trapped waves off the west coast of the United States, Summer 1973. *J. Phys. Oceanogr.*, **6**, 856–864.
- Weickmann, K. M., 1983: Intraseasonal circulation and outgoing longwave radiation modes during northern hemisphere winter. *Mon. Wea. Rev.*, **111**, 1838–1858.
- , G. R. Lussky and J. E. Kutzback, 1985: Intraseasonal (30–60 day) fluctuations of outgoing longwave radiation and 250 mb streamfunction during northern winter. *Mon. Wea. Rev.*, **113**, 942–961.
- Yao, T., H. J. Freeland and L. A. Mysak, 1984: A comparison of low-frequency current observations off British Columbia with coastal trapped wave theory. *J. Phys. Oceanogr.*, **14**, 22–34.